DESIGN AND TESTING OF AN AIR SUCTION ORCHARD FRUIT-BAG COLLECTION MACHINE
/
气吸式果园套袋纸回收机设计与试验

Caiqi HU[1,2], Junbo WANG[1,2], Fengjie TENG[1,2], Rendong SUI*[1,2]
[1] College of Mechanical and Electrical Engineering, Qingdao Agricultural University, Shandong / China;
[2] Shandong Provincial Key Laboratory of Smart Agricultural Equipment for Protected Horticulture / China
Tel: 8613475835919; E-mail: 827435160@qq.com
Corresponding author: Rendong SUI
DOI: https://doi.org/10.35633/inmateh-79-111

***Keywords:** orchard fruit-bag collection; air suction; airflow field analysis; orchard field test*

ABSTRACT
To address the environmental pollution caused by discarded non-biodegradable fruit bags in orchards, an air-suction orchard fruit-bag collection machine was developed. First, theoretical calculations and analyses were conducted on the key machine components to determine the main operating parameters. Kinematic analysis was then performed using ADAMS, and the airflow field was simulated using Fluent. Next, a prototype was manufactured. Based on multivariable response surface analysis conducted in Design-Expert, the optimal parameter combination was identified as a travel speed of 2 km/h, a suction-inlet air velocity of 15.5 m/s, and a helical-conveyor rotational speed of 66 r/min. Orchard field tests showed that, under the optimal operating conditions, the actual collection rate reached 82.5%, confirming that the machine met the intended design requirements.

摘要
针对果园废弃套袋纸不易降解、污染环境等问题，提出了气吸式果园套袋纸回收机的设计。首先对关键装置进行理论计算与分析，确定影响作业效果的关键因素，以此为基础进行 ADAMS 运动学分析和 Fluent 气流场仿真分析。然后进行样机研制，通过 Design-Expert 进行多因素响应面分析，确定整机的工作参数最佳组合为：行进速度为 2 km/h、吸入口风速为 15.5 m/s、螺旋输送装置转速为 66 r/min。果园试验表明，在最佳工作参数下，样机试验回收率为 82.5%, 验证本设计能够实现预期的工作效果。

INTRODUCTION
The bagging of young fruit on trees has been widely adopted in orchards for crops such as apples, pears, and peaches. Taking apple orchards as an example, fruit bags not only help reduce pest and disease incidence and limit pesticide exposure but also significantly improve fruit appearance and quality *(Liu et al., 2024; Yu et al., 2022)*. To promote uniform coloration, the bags are generally removed approximately two weeks before harvest, after which they are often discarded in the orchard *(Hong et al., 2020; Kim et al., 2013)*. Because these fruit bags are primarily made from wood pulp with a high fiber content and also contain wet-strength agents and other additives, their natural degradation is limited *(Chen et al., 2024)*. Therefore, collecting the discarded fruit bags can reduce resource waste and help protect the orchard production environment *(Luo et al., 2011; Zhang et al., 2014)*.

Currently, waste fruit bags are collected primarily by hand, a process characterized by high labor requirements, high costs, and low efficiency. These limitations reduce orchard growers' willingness to participate in collection activities *(He et al., 2022; Cao et al., 2019)*. The lack of efficient mechanical collection equipment has therefore become a major constraint on the sustainable development of the fruit industry *(Cai et al., 2024; Bishnoi et al., 2023)*. Research on machinery specifically designed to collect discarded fruit bags in orchards remains limited both in China and internationally; however, relevant studies have been conducted on related collection equipment.

For example, Guo Wensong of China Agricultural University developed a brush-tooth mechanically driven film-separation device for collecting residual plastic film *(Guo et al., 2020; Wang et al., 2019)*. The brush teeth dislodged the residual film, after which negative-pressure airflow at the suction inlet lifted the film.

The collected material was then discharged by a centrifugal fan and separated using a mesh screen. In addition, Liu Enshui and colleagues at Tarim University used Fluent to simulate a gravity settling chamber and determine the optimal operating parameters of the collection device *(Liu et al., 2021; Wang et al., 2012)*.

Existing studies have focused mainly on residual-film collection machinery *(Peng et al., 2020; Hou et al., 2023; Wang et al., 2024)*, whereas research specifically addressing air-suction machines for collecting discarded fruit bags remains limited *(Ken et al., 2024; Ma et al., 2024)*. Although several machines based on relatively simple operating principles have been investigated, innovation in their collection mechanisms has been insufficient, limiting their ability to meet the practical requirements of large-scale discarded fruit-bag collection.

To address these challenges, an air-suction orchard fruit-bag collection machine was developed. The key components were analyzed theoretically to determine the main operating parameters. Kinematic simulations were then conducted in ADAMS, and computational fluid dynamics simulations were performed in Fluent to evaluate the mechanical and aerodynamic performance of the machine. A prototype was subsequently manufactured based on the theoretical analysis and simulation results. Response surface methodology was used to determine the optimal combination of operating parameters, with the collection rate selected as the response variable. Experimental results confirmed that the machine met the intended design requirements.

MATERIALS AND METHODS

Physical Characteristics of Discarded Fruit Bags

The physical characteristics of discarded fruit bags from apple orchards were determined through systematic sampling. A total of 100 discarded fruit bags were randomly collected and divided equally into 10 groups for statistical analysis. Their main physical properties were as follows: the mean length was 180 mm, the mean width was 147 mm, and the mean thickness was 2.2 mm. The coefficient of friction and the mean mass of a single bag were 0.52 and 5.6×10^{-3} kg, respectively. Representative fruit bags are shown in Fig. 1.

The terminal velocities of the fruit bags ranged from 2.9 to 5.6 m/s, whereas those of soil-clod impurities ranged from 11.5 to 15.0 m/s.

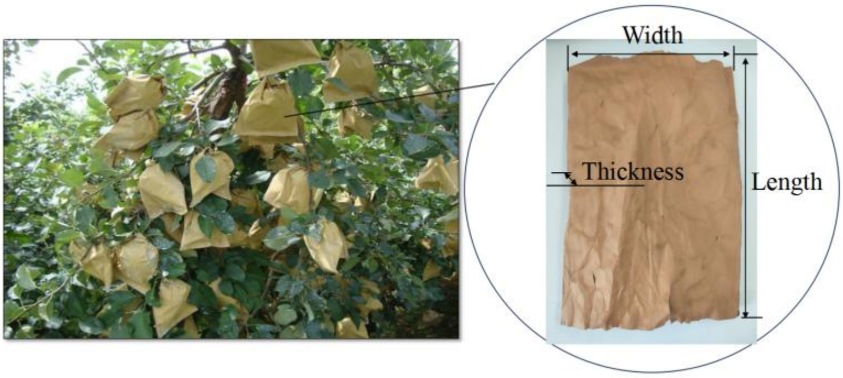

(a) Fruit bags on an apple tree (b) Enlarged view of a fruit bag

Fig. 1- Fruit bags and their dimensional characteristics

Overall Structure and Operating Principle

The air-suction fruit-bag collection machine mainly consists of a centrifugal fan, an air duct, a settling chamber, a helical conveyor, a direction-changing mechanism, a vertical scraper, a filter screen, a compression device, an engine, and a transmission system. The overall structure of the machine is shown in Fig. 2.

Power is transmitted from the power take-off shaft to the centrifugal fan through a belt-and-pulley drive, while the helical conveyor and vertical scraper are driven by chain-and-sprocket mechanisms. The rotating blades on both sides of the vertical scraper move the fruit bags toward the center, after which the helical conveyor further conveys them to the central collection area. A filter screen mounted at the bottom provides preliminary removal of impurities. The negative-pressure airflow generated by the centrifugal fan then draws the concentrated fruit bags into the settling chamber, where larger impurities are separated.

The cleaned fruit bags are subsequently conveyed through the air duct to the collection bin. Finally, the compression device compacts the bags, thereby completing the collection process.

The vertical scraper, helical conveyor, and settling chamber are the key components of the air-suction fruit-bag collection machine. Accordingly, the design and analysis of these components constitute the main focus of this study.

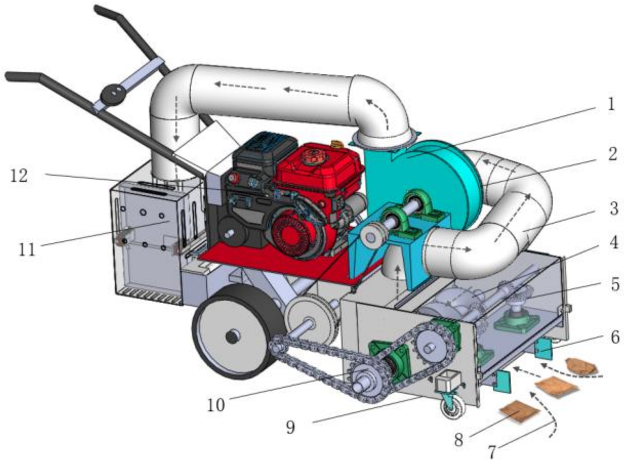

Fig. 2 - Structure of the air-suction fruit-bag collection machine

1. Centrifugal fan; 2. Air duct; 3. Settling chamber; 4. Helical conveyor; 5. Direction-changing mechanism; 6. Vertical scraper; 7. Fruit-bag trajectory; 8. Fruit bag; 9. Filter screen; 10. Transmission system; 11. Compression device; 12. Engine.

Design of the Vertical Scraper Collection Mechanism

The vertical scraper collection mechanism mainly consists of a horizontal drive shaft, two vertical rotating shafts, an adjustment plate, bearing housings, and two symmetrically arranged vertical scraper blades connected through a reversing mechanism. Power is supplied by the engine, and the rotational speed is reduced through belt, chain, and bevel-gear transmissions. The two meshing bevel-gear pairs rotate in opposite directions, ensuring that the left and right scraper blades move the fruit bags toward the center.

The operating principle of the vertical scraper collection mechanism is shown in Fig. 3. Power is transmitted to the horizontal drive shaft through a chain drive, causing the shaft to rotate clockwise. A small bevel gear mounted on the drive shaft engages with a large bevel gear, thereby driving the scraper blades on both sides to rotate inward and move the fruit bags toward the center. To ensure stable fruit-bag collection, an appropriate rotational speed of the scraper blades must be determined.

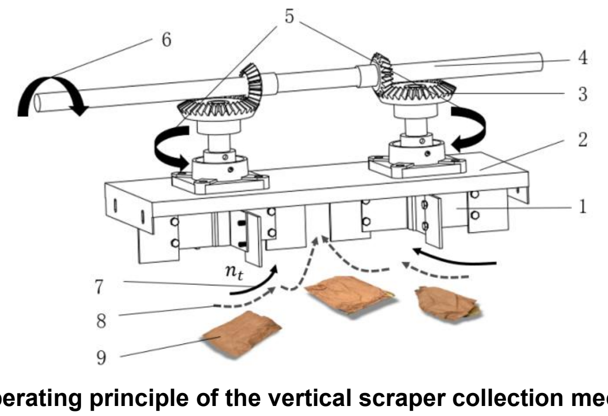

Fig. 3 - Operating principle of the vertical scraper collection mechanism

1. Scraper blades; 2. Adjustment plate; 3. Direction-changing mechanism; 4. Horizontal drive shaft; 5. Rotation direction of the vertical shafts; 6. Rotation direction of the drive shaft; 7. Rotation direction of the scraper blades; 8. Fruit-bag trajectory; 9. Fruit bag.

During operation, the vertical scraper collection mechanism relies primarily on the centrifugal force generated by the rotating scraper blades to move the fruit bags toward the center. A force analysis was conducted for the scraper blade, fruit bag, and bottom plate, and a rectangular coordinate system was established, as shown in Fig. 4. At the position illustrated, the fruit bag is subjected to the centrifugal force exerted by the scraper blade, the friction force acting along the bottom plate, the normal support force from the bottom plate, and its own weight.

Force equilibrium along the bottom plate indicates that the fruit bag can be conveyed into the collection mechanism only when the component of centrifugal force in the conveying direction exceeds the sum of the friction force and the component of gravity acting along the bottom plate.

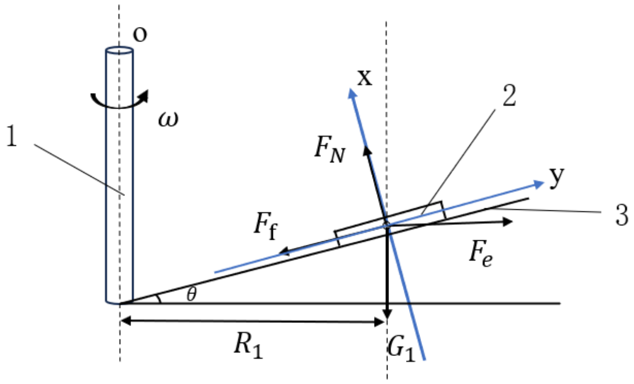

Fig. 4 - Force analysis of a fruit bag on the bottom plate

1. Vertical rotating shaft; 2. Fruit bag; 3. Bottom plate.

Force analysis:

$$\begin{cases} F_f + G_1 \sin\theta \le F_e \cos\theta \\ F_N = G_1 \cos\theta + F_e \sin\theta \end{cases} \tag{1}$$

where:

$$G_1 = m_l g \tag{2}$$

$$F_f = \mu F_N = \mu(m_l g \cos\theta + F_e \sin\theta) \tag{3}$$

where, F_e is the centrifugal force acting on the fruit bag, N; F_f is the friction force acting on the fruit bag, N; G_1 is the weight of the fruit bag, N; F_N is the normal support force exerted by the bottom plate, N; m_l is the mass of a single fruit bag, kg ; θ is the inclination angle of the bottom plate, set to 7°; μ is the coefficient of friction between the fruit bag and the bottom plate, set to 0.52.

Based on the measured physical characteristics, the mass of a single fruit bag was 5.6×10^{-3} kg. Substitution of the relevant parameters into Eqs. (1)–(3) showed that the centrifugal force acting on the fruit bag must exceed 3.77×10^{-2} N for the bag to be conveyed smoothly along the bottom plate and into the collection mechanism.

The centrifugal force generated during blade rotation is related to the blade rotational speed as follows:

$$F_e = m_l \omega_t^2 R_1 \tag{4}$$

$$\omega_t = \frac{\pi n_t}{30} \tag{5}$$

where, ω_t is the angular velocity of the scraper blades, rad·s⁻¹; R_1 is the radial distance from the axis of rotation to the fruit bag, m; n_t is the rotational speed of the scraper blades, r·min⁻¹.

The minimum centrifugal force required for successful collection by the vertical scraper mechanism was calculated to be 3.77×10^{-2} N. According to Eqs. (4) and (5), when the blade radius was 0.18 m, the corresponding rotational speed of the scraper blades was 58.39 r·min⁻¹. Therefore, the vertical scraper mechanism can collect the fruit bags smoothly when the blade rotational speed exceeds 58.39 r·min⁻¹.

Design of the Helical Conveyor

To convey the fruit bags toward the center of the machine, a helical conveyor was designed. Helical blades were welded symmetrically to both sides of a hollow shaft, with equal numbers of blades arranged in opposite helical directions. Arc-shaped baffles closely followed the curvature of the rotating blades, thereby helping to prevent fruit-bag accumulation. A filter screen mounted at the bottom removed impurities such as weeds and soil clods. As shown in Fig. 5, the helical conveyor mainly consists of a hollow shaft, helical blades, arc-shaped baffles, a filter screen, and shock-absorbing wheels.

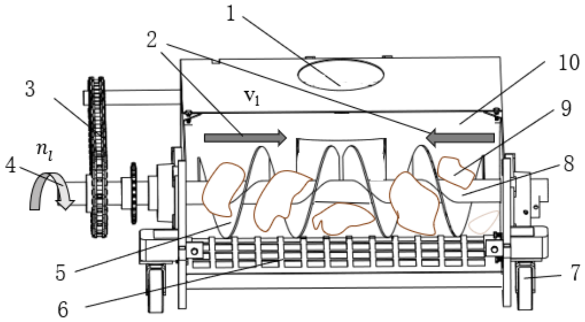

Fig. 5 - Structure and operating principle of the helical conveyor

1. Fruit-bag inlet; 2. Direction of fruit-bag movement; 3. Chain. 4. Rotation direction of the hollow shaft; 5. Helical blades; 6. Filter screen. 7. Shock-absorbing wheel. 8. Hollow shaft. 9. Fruit bag. 10. Arc-shaped baffle.

Based on the operating requirements of the collection machine, the principal geometric parameters of the helical blades were designed, including the outer diameter D_l, shaft diameter d_l, and pitch S_l.

To ensure that the fruit bags entered the helical conveyor smoothly and were conveyed from both sides toward the center, the helical-blade dimensions were selected according to the measured dimensions of the fruit bags. The structural parameters of the conveyor were determined with reference to the fruit-bag characteristics and the *Agricultural Machinery Design Manual*. Considering the physical properties of the fruit bags and the orchard operating environment, the blade outer diameter D_l, pitch S_l, and shaft diameter d_l were set to 160, 160, and 40 mm, respectively, to improve conveying efficiency.

During operation, an excessively low rotational speed of the helical blades may prevent the fruit bags from being conveyed promptly toward the center, resulting in accumulation on both sides. Conversely, an excessively high rotational speed may cause the blades to strike the bags, making them bounce and disrupting their movement toward the center. This may cause the bags to fall out of the conveying area. Therefore, the critical rotational speed of the helical conveyor must be determined.

To prevent accumulation and bouncing, the rotational speed of the helical conveyor should be maintained between the minimum speed required for effective conveying and the critical speed at which the fruit bags begin to lose stable contact with the conveyor. The critical condition was determined by comparing the centrifugal force acting on a fruit bag with its weight:

$$\frac{m_l \omega_l^2 D_l}{2} \le m_l g \tag{6}$$

where:

$$\omega_l = \frac{\pi n_l}{30} \tag{7}$$

where, m_l is the mass of a single fruit bag, kg; ω_l is the angular velocity of the helical conveyor, rad·s⁻¹; g is the gravitational acceleration, m·s⁻²; n_l is the rotational speed of the helical blades, r·min⁻¹.

Substituting Eq. (6) into Eq. (7) gives:

$$n_l \le \frac{30}{\pi}\sqrt{\frac{2g}{D_l}} \tag{8}$$

The calculated critical rotational speed of the helical blades was 106.76 r·min⁻¹. Therefore, considering the previously determined minimum operating speed, the helical conveyor should operate within the range of 58.39–106.76 r·min⁻¹. Within this range, the conveyor can meet the requirements for stable fruit-bag conveying and collection while reducing the risks of blockage and bag bouncing.

Kinematic Simulation of the Helical Conveyor

To evaluate the conveying performance of fruit bags in the helical conveyor, a kinematic simulation was conducted using ADAMS. Before analyzing the motion of the conveyor, kinematic constraints between the components and contact constraints between the fruit bags and the relevant machine parts were defined in the model. The simulation duration was set to 8 s, with 500 calculation steps. The constraint relationships are listed in Table 1. Because the shape of the fruit bags varied, three representative bag shapes were included in the simulation, as shown in Fig. 6.

Table 1

Constraint relationships in the helical conveyor model

No.	Constraint type	Constrained components
1	Fixed joint	Frame–ground
2	Fixed joint	Helical blades–auger shaft
3	Revolute joint	Auger shaft–frame
4	contact	Fruit bag–frame
5	contact	Fruit bag–helical blades
6	contact	Fruit bag–auger shaft

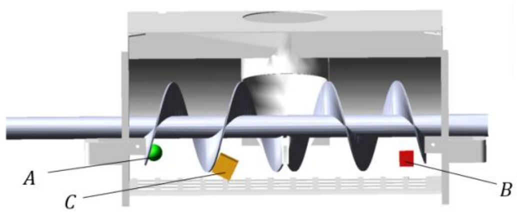

Fig. 6 - ADAMS model of the helical conveyor and representative fruit-bag shapes

A, fruit bag 1, B, fruit bag 2, C, fruit bag 3.

Based on the simulation results, the displacement curves of the fruit bags at different helical-blade rotational speeds are shown in Fig. 7.

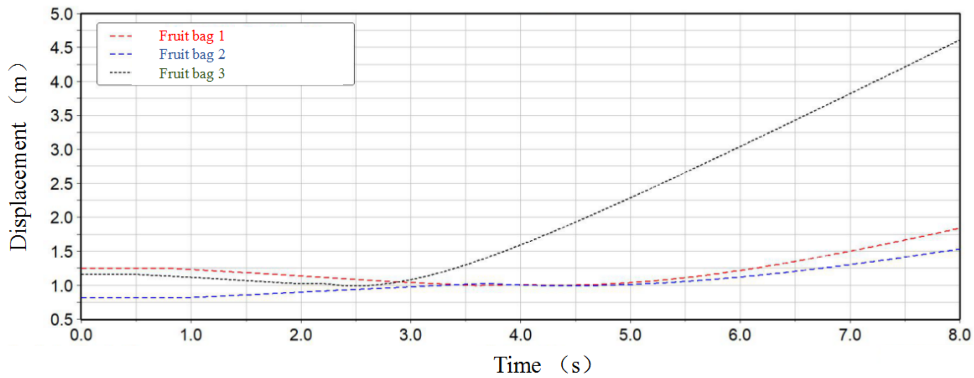

(a) Helical-blade rotational speed of 58.39 r·min⁻¹

(b)

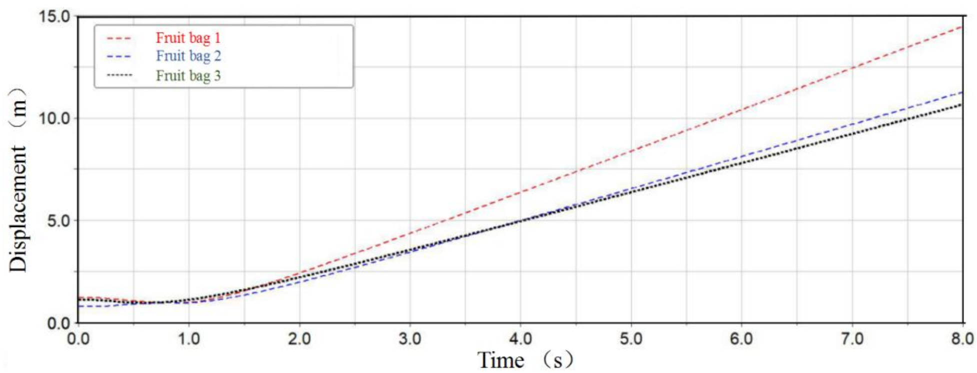

(b) Helical-blade rotational speed of 106.76 r·min⁻¹

Fig. 7 - Displacement curves of the fruit bags at different helical-blade rotational speeds

As shown in Fig. 7, comparison of the displacement curves at helical-blade rotational speeds of 58.39 and 106.76 r·min⁻¹ indicates that a higher rotational speed produced greater fruit-bag displacement over the same period. All three representative fruit bags exhibited stable and smooth motion. These results demonstrate that the helical conveyor can reliably convey the fruit bags toward the center of the machine.

Design of the Settling Chamber

The settling chamber uses gravity-induced settling to separate fruit bags from impurities. It plays an important role in both fruit-bag recovery and impurity removal. The chamber mainly consists of a settling section, an inlet, and an outlet. Its structure and operating principle are shown in Fig. 8.

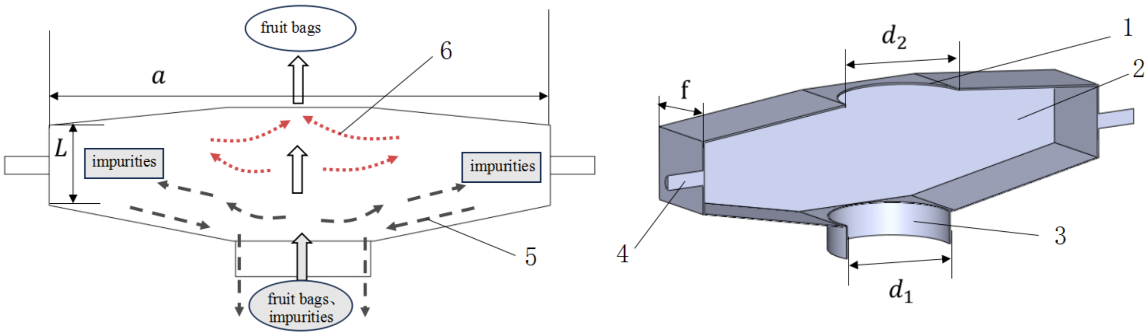

Fig. 8 - Structure and operating principle of the settling chamber

1. Air outlet; 2. Settling section; 3. Inlet; 4. Fixed shaft; 5. Impurity trajectory; 6. Fruit-bag trajectory.
a, length of the settling chamber; f, half-width of the settling chamber; L, height of the settling chamber;
d_1 is the inlet diameter; d_2, air-duct diameter.

Field investigations showed that, during fruit-bag collection, brittle weed residues were broken into smaller fragments by the vertical scraper and helical conveyor and were subsequently removed through the bottom filter screen. Only a small amount of large weed material entered the settling chamber. Therefore, the impurities reaching the settling chamber consisted mainly of small soil clods. To achieve effective separation of the fruit bags from the soil clods, the airflow velocity in the settling chamber had to be higher than the terminal velocity of the fruit bags but lower than that of the soil clods.

Assuming a constant volumetric airflow rate through the system, different airflow velocities can be obtained by designing the inlet and settling section with different cross-sectional areas. The corresponding airflow velocities were calculated using Eq. (9):

$$Q = v_1 A_1 = v_2 ab \tag{9}$$

where, Q is the volumetric airflow rate supplied by the centrifugal fan, m³·s⁻¹; v_1 is the airflow velocity at the inlet, m·s⁻¹; A_1 is the cross-sectional area of the inlet, m²; is the airflow velocity in the settling section, m·s⁻¹; *a* and *b* are the length and width of the settling section, respectively, m.

Considering that the mean fruit-bag length was 180 mm and that sufficient clearance was required for pneumatic conveying, both the air-duct diameter and the inlet diameter were set to 200 mm. Based on the measured terminal velocities of the fruit bags and soil clods, the airflow velocity in the settling chamber was set to 5.6 m·s⁻¹ to facilitate impurity separation. The settling-chamber length was set to 500 mm so that it was compatible with the overall dimensions of the collection mechanism. According to Eq. (9), the required settling-chamber width was calculated to be 224 mm.

Because the cross-sectional area gradually increased from the suction inlet to the settling chamber, the airflow velocity decreased through this transition region, thereby reducing the aerodynamic force acting on both the fruit bags and the soil clods. Effective separation occurred when the aerodynamic lifting force was sufficient to entrain the fruit bags but insufficient to carry the soil clods. Under these conditions, the fruit bags were conveyed upward by the airflow, whereas the soil clods settled under gravity and were discharged through the bottom screen rather than entering the collection bin. The resultant force acting on a soil clod is expressed by Eq. (10):

$$F = Kmv_2^{\ 2} - mg = Kmv_2^{\ 2} - Kmv_t^{\ 2} = ma_1 \tag{10}$$

where, F is the resultant force acting on the soil clod, N; m is the mass of the soil clod, in kilograms，kg; g is the gravitational acceleration, taken as 9.8 m·s⁻²; K is the aerodynamic or buoyancy coefficient of the soil clod; v_t is the terminal velocity of the soil clod, m·s⁻¹; a_1 is the acceleration of the soil clod, m·s⁻².

As the aerodynamic lifting force gradually decreased, the soil clods moved upward under deceleration until their velocity decreased to zero, with the resultant acceleration being non-positive.

The upward travel distance of the soil clods was used to determine the required height of the settling chamber. This distance is expressed by Eq. (11):

$$-{v_3}^2 = 2a_1h \tag{11}$$

where, h is the upward travel distance of the soil clod, m; v_3 is the initial upward velocity of the soil clod at the bottom of the settling chamber, m·s⁻¹.

Based on the structural requirements of the machine, the initial velocity of the soil clod at the bottom of the settling chamber was set to 5.6 m·s⁻¹. Substitution of the relevant parameters into Eq. (11) yielded a required settling-chamber height of 123 mm.

Airflow-Field Simulation Analysis of the Settling Chamber

The airflow field in the fruit-bag conveying system is highly complex. To characterize the airflow behavior, simulation analysis was conducted using Fluent. Velocity distributions were analyzed on cross-sections of both the settling chamber and the conveying duct, allowing the transport behavior of the fruit bags to be observed visually.

The measured terminal velocity of the fruit bags ranged from 2.9 to 5.6 m·s⁻¹. According to the empirical coefficient, the conveying airflow velocity should be 2.6-5.0 times the terminal velocity of the fruit bags. Considering the practical operating conditions and the need for impurity removal, the inlet airflow velocity should not be set excessively high. Based on a comprehensive assessment, inlet velocities of 15, 16, and 17 m·s⁻¹ were selected. The simulated airflow-velocity contours under these three inlet conditions are shown in Fig. 9.

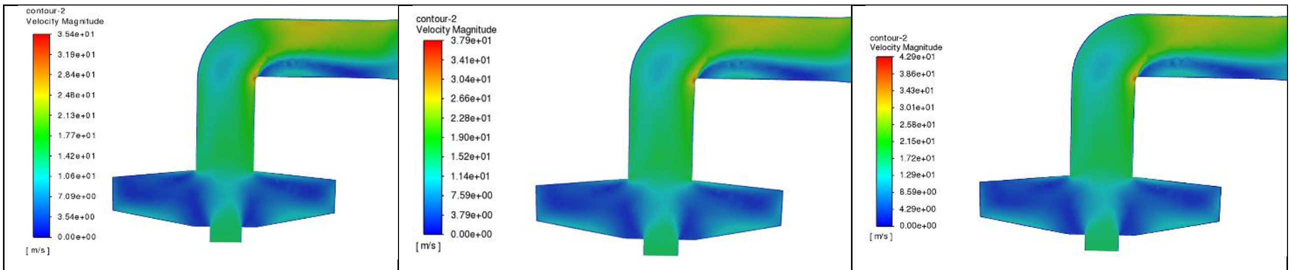

(a) Inlet velocity of 15 m·s⁻¹ | (b) Inlet velocity of 16 m·s⁻¹ | (c) Inlet velocity of 17 m·s⁻¹

Fig. 9 - Airflow-velocity contours at different inlet velocities

As shown in Fig. 9(a), at an inlet velocity of 15 m·s⁻¹, the airflow velocity near the lower section of the settling chamber reached approximately 17 m·s⁻¹, allowing the fruit bags and impurities to be rapidly drawn into the chamber. As the cross-sectional area of the settling chamber increased, the airflow velocity gradually decreased from the central region toward both ends. The velocity at both ends was approximately 5.6 m·s⁻¹, which facilitated separation of the fruit bags from the impurities. In the upper section of the settling chamber, the cross-sectional area decreased abruptly, causing the airflow velocity to increase to approximately 18 m·s⁻¹ and enabling the fruit bags to be conveyed smoothly through the outlet.

As shown in Fig. 9(b), the conveying performance at an inlet velocity of 16 m·s⁻¹ was similar to that observed at 15 m·s⁻¹. Under this condition, the fruit bags were effectively separated from the impurities and conveyed smoothly through the outlet.

As shown in Fig. 9(c), when the inlet velocity was set to 17 m·s⁻¹, the airflow velocity near the lower section of the settling chamber reached approximately 21 m·s⁻¹, allowing both the fruit bags and impurities to enter the chamber. However, the airflow velocity in the middle section ranged from 8.59 to 12.9 m·s⁻¹. This range exceeded the terminal velocity of the soil-clod impurities, resulting in incomplete separation of the impurities from the fruit bags.

Based on these results, the inlet airflow velocity should be maintained between 15 and 16 m·s⁻¹ to ensure effective separation of the fruit bags from impurities and stable conveying through the system.

RESULTS

Orchard Field Test

Based on the preceding design and simulation analyses, a prototype was manufactured and tested in an apple orchard. The tree-row spacing ranged from 1,400 to 2,000 mm, while the within-row tree spacing ranged from 1,100 to 1,400 mm. The machine travel speed was varied from 1 to 3 km·h⁻¹. The orchard field test is shown in Fig. 10.

Fig. 10 - Orchard field test of the prototype

Experimental Design and Parameter Optimization

To determine the optimal combination of operating parameters, a three-factor, three-level response surface experiment was designed using Design-Expert. The selected test factors were machine travel speed (1~3 km·h⁻¹), inlet airflow velocity (15~16 m·s⁻¹), and *helical-conveyor* rotational speed (62~68 r·min⁻¹). The coded levels of these factors are presented in Table 2. The fruit-bag collection rate was selected as the response variable and was calculated as follows:

$$Y_1 = (1 - \frac{M_2}{M_1}) \times 100\% \tag{12}$$

where, Y_1 is the fruit-bag collection rate, %; M_2 is the mass of fruit bags remaining in the field after operation, kg; M_1 is the initial mass of fruit bags in the field before operation, kg.

Table 2

Coded levels of the experimental factors

Coded level	Factors		
	Travel speed (km·h⁻¹)	Inlet airflow velocity (m·s⁻¹)	Helical-conveyor rotational speed (r·min⁻¹)
-1	1	15	62
0	2	15.5	65
1	3	16	68

According to the experimental design, 17 experimental runs were conducted. The experimental design matrix and corresponding results are presented in Table 3. In the table, X_1, X_2, and X_3 represent the coded values of the three factors, while Y_1 denotes the fruit-bag collection rate.

Table 3

Experimental design matrix and collection-rate results

Run	Factors			Fruit-bag collection rate Y_1/%
	Travel speed X_1	Inlet airflow velocity X_2	Helical-conveyor rotational speed X_3	
1	1	1	0	74.8
2	0	0	0	83.5

Run	Factors			Fruit-bag collection rate Y_1/%
	Travel speed X_1	Inlet airflow velocity X_2	Helical-conveyor rotational speed X_3	
3	0	0	0	82
4	0	1	-1	78.1
5	1	-1	0	72.7
6	-1	-1	0	74.5
7	-1	0	1	80
8	0	-1	1	82.1
9	0	-1	-1	78.9
10	0	0	0	83.1
11	-1	1	0	71
12	1	0	1	78.5
13	0	0	0	82.7
14	0	0	0	83
15	1	0	-1	75.2
16	0	1	1	80.7
17	-1	0	-1	78.4

Multiple regression analysis was performed on the experimental data, and the analysis of variance (ANOVA) results are presented in Table 4. The overall regression model was highly significant (P < 0.05), whereas the lack of fit was not significant (P > 0.05), indicating that the model adequately described the experimental data. The terms X_3, X_1^2, and X_2^2 had highly significant effects on the fruit-bag collection rate. According to the reported P-values, X_1, X_2, and the interaction term X_1X_2 also had significant effects, whereas the remaining terms were not significant. Based on the reported main-effect results, the factors were ranked in descending order of their influence on the collection rate, Y_1, as follows: helical-conveyor rotational speed (X_3), inlet airflow velocity (X_2), and machine travel speed (X_1).

Table 4

Analysis of variance for the regression model of fruit-bag collection rate

Source	Collection rate				
	Sum of squares	df	Mean Square	*F*-value	*P*-value
model	238.81	9	26.53	26.37	< 0.0001**
X_1	0.9112	1	0.9112	0.9055	0.037*
X_2	1.62	1	1.62	1.61	0.024*
X_3	14.31	1	14.31	14.22	0.007**
X_1X_2	7.84	1	7.84	7.79	0.0269*
X_1X_3	0.7225	1	0.7225	0.7179	0.4248
X_2X_3	0.09	1	0.09	0.894	0.7736
X_1^2	140.06	1	140.06	139.17	< 0.0001**
X_2^2	62.17	1	62.17	61.77	< 0.0001**
X_3^2	3.66	1	3.66	3.64	0.0981
Residual	7.04	7	1.01		
Lack of fit	5.79	3	1.93	6.17	0.0556
Pure error	1.25	4	0.313		
Total	245.85	16			

Note: * Significant at (0.01≤P≤0.05); ** highly significant at (P<0.01).

To provide a more intuitive representation of the interaction effects of the factors on the fruit-bag collection rate, the response surface was generated from the experimental results and the regression model, as shown in Fig. 11. When the machine travel speed was held constant, the collection rate first increased and then decreased as the inlet airflow velocity increased, reaching a maximum when the inlet airflow velocity ranged from 15.2 to 15.8 m·s⁻¹. In addition, the collection rate reached its highest value when the machine travel speed ranged from 1.5 to 2.5 km·h⁻¹.

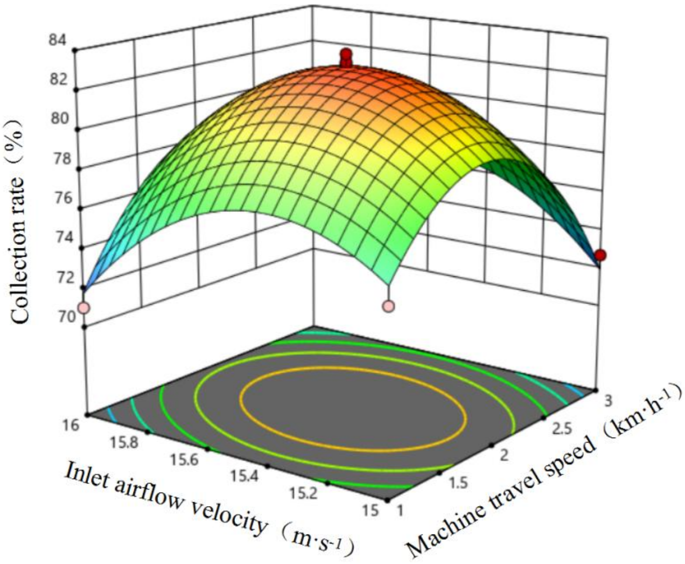

Fig. 11 - Effects of travel speed and inlet airflow velocity on the fruit-bag collection rate

Based on the ANOVA and response surface analyses, the regression equation for the fruit-bag collection rate, Y_1, was obtained as follows:

$$Y_1 = 82.86 - 0.3375X_1 - 0.45X_2 + 1.34X_3 + 1.4X_1X_2 - 5.77X_1^2 - 3.84X_2^2 \quad (13)$$

Considering the operating requirements of the air-suction fruit-bag collection machine, Design-Expert was used to optimize Eq. (13). The optimal parameter combination was a machine travel speed of 1.895 km·h⁻¹, an inlet airflow velocity of 15.509 m·s⁻¹, and a helical-conveyor rotational speed of 66.22 r·min⁻¹. Under these conditions, the model predicted a collection rate of 83.5%.

Experimental Results

The optimized parameters were rounded to practical operating values of 2 km·h⁻¹ for machine travel speed, 15.5 m·s⁻¹ for inlet airflow velocity, and 66 r·min⁻¹ for helical-conveyor rotational speed. Ten orchard field-test runs were conducted under these conditions. The mean collection rate was 82.5%, and the relative error between the predicted and measured values was 1.21%. The close agreement between the two values confirmed the reliability of the optimization model.

CONCLUSIONS

This study systematically investigated the environmental pollution caused by discarded fruit bags in orchards and their potential for recovery. An air-suction fruit-bag collection machine was designed, simulated, manufactured, and experimentally validated. The main conclusions are as follows:

(1) Based on the structural design and theoretical calculations, kinematic simulations of the helical conveyor were conducted using ADAMS, and airflow-field simulations of the settling chamber were performed using Fluent. The results showed that when the inlet airflow velocity ranged from 15 to 16 m·s⁻¹, the fruit bags could be effectively separated from the impurities and conveyed smoothly through the collection system.

(2) A prototype was manufactured based on the theoretical calculations and simulation results, and orchard field tests were conducted. Design-Expert was used to determine the optimal operating parameters. Under the optimized conditions, the measured collection rate was 82.5%. The field-test results confirmed that the machine met the intended design requirements.

ACKNOWLEDGEMENT

This research was funded by the National Natural Science Foundation of China (No: 31971801), the Natural Science Foundation of Shandong Province of China (No: ZR2020ME252, ZR2020ME250), Qingdao Science and Technology Benefit-the-People Demonstration Project (No: 25-1-5-xdny-33-nsh), and the University-enterprise Cooperation Project (No: H20250184).

REFERENCES

[1] Bishnoi, M., Goyal, K, R., Vats, C., Singla, A., (2023). Effect of Pre-Harvest Fruit Bagging on Fruit Quality Characteristics of Different Guava Cultivars during Rainy Season. *International Journal of Plant Soil Science*, 35 (21): 63-71.

[2] Cai, J., Zhang, J., Gao, Z., Wang, X., Guo, G., Baikeli, Y., Tang, X., Wang, Y., (2024). Design and test of a wheel-belt type cotton stalk puller(轮带式棉秆拔取装置的设计与试验). *Int J Agric & Biol Eng*, 17 (2): 102–108.

[3] Cao, C., Luo, K., Peng, M., Wu, Z., Liu, G., Li, Z., (2019). Experimental on winnowing mechanism and winnowing performance of hickory material (山核桃物料风选机理与风选性能试验研究).*Transactions of the Chinese Society for Agricultural Machinery*, 50 (09): 105-112.

[4] Chen,Y; Xing, R.; Liu, X.; Zhang, H.; Li, H. (2024). Design and Test of Potato Seedling Killing and Residual Film Recycling Integrated Machine(马铃薯杀秧与残膜回收联合作业机的设计与试验). *Agronomy*, 14, 2269.

[5] Guo, W., He, X., Wang, L., Zhao, P., Hu, C., Hou, S., Wang X., (2020). Development of a comb tooth loosening and pneumatic stripping plough layer residual film recovery machine (梳齿起膜气力脱膜式耕层残膜回收机研制). *Transactions of the Chinese Society of Agricultural Engineering (Transactions of the CSAE)*, 36 (18): 1-10.

[6] He, J., Cheng, X, T., Gao, Y., Zhang, X., Jia, X., (2022). Comparison of quality and storability among bagged and non-bagged fruits of three apple varieties (3 个苹果品种套袋果与不套袋果品质及耐贮性的比较). *China Fruits*, (06): 6-9.

[7] Hong K L, Sang H Y. (2020). Machine Learning Feature Extraction Based on Binary Pixel Quantification Using Low-Resolution Images for Application of Unmanned Ground Vehicles in Apple Orchards (基于低分辨率图像二值像素量化的机器学习特征提取方法及其在苹果园无人地面车辆中的应用). *Agronomy*, 10 (12): 1926-1926.

[8] Hou, G., Chen, H., Jiang, M., Niu, R., (2023). An Overview of the Application of Machine Vision in Recognition and Localization of Fruit and Vegetable Harvesting Robots. *Agriculture*, 13, 1814.

[9] Ken, T., Daisuke, S., Sadayuki, K., (2024). Comparison of performance between tapered and cylindrical roller bearings for pinion of gear unit subjected to rotation test. *Proceedings of the Institution of Mechanical Engineers*, 238 (3): 332-344.

[10] Kim, K., Lee, M., Eom, T., (2013). Preparation of Emulsion from Biodegradable Polymer (II) - Characteristics of paper treated as PLA and PBS emulsion. *Journal of Korea Technical Association of the Pulp and Paper Industry*, 45 (2): 13-20.

[11] Liu, E., (2021). Optimal design of residual film recovery machine with comb-tooth film lifting and pneumatic film stripping(梳齿式起膜与气力脱膜残膜回收机的优化设计).*Tarim University*.

[12] Liu, X., Ma, T., Zhang, H., Yan, K., Zhou, S., (2024). The accumulation of fungal not bacterial residue carbon is management-dependent under conventional and organic practices in apple-orchard soil. *Geoderma*, 448: 116968-116968.

[13] Luo, Y., Zhang, M, Y., Wang, J., (2011). Comparison experiment of three sizing agents of fruit-bagged paper(三种果袋纸施胶剂的对比实验研究). *Paper and Paper Making*, 30 (06): 6.

[14] Ma, Z., Zhu, Y., Li, J., Song, Z., Yu, J., Li, Y., Xu, L., (2024). Study on the performance of detection air duct and evaluation index of agricultural cleaning centrifugal fans(农用清洁离心风机检测风道性能及评价指标研究). *Biosystems Engineering*, 23981-97.

[15] Peng, Q., Li, C., Kang, J., Shi, G., Zhang, H., (2020). Improved design and test on Pneumatic cylinder sieve Film Hybrid Separator(气力式圆筒筛膜杂分离机改进设计与试验). *Transactions of the Chinese Society for Agricultural Machinery*, 51 (08): 126-135.

[16] Wang, H., Sun, W., Wang, H., Simionescu, P.A. (2024). Automated Mulched Transplanting of Angelica Seedlings Using a Pneumatic Sowing Device. *Agronomy*, 14, 3076.

[17] Wang, J., Xie, H., Li, G., Yan, J., Wei, H., Wu, H. (2019). Design and Simulation of Airflow Uniformity Mechanism for Fixed-Bed Peanut Pod Drying Equipment （固定床式花生荚果烘干设备匀风机构设计与仿真）. *Chinese Journal of Agricultural Machinery and Chemistry*, 40 (04): 84-92.

[18] Wang, W., Wang, C., (2012). Parameter Analysis and Simulation of Toothed Roller Pickup Device(弹齿滚筒式捡拾装置参数分析与仿真). *Transactions of the Chinese Society for Agricultural Machinery*, 43 (10): 82-89.
[19] Yu, M., Wen, Y., Mao, M., (2022). The pattern and development trend of China's apple foreign trade（我国苹果对外贸易格局及发展趋势）. *China Fruits*, (07): 100-104.
[20] Zhang, M., Liu, Y., Wang, X., (2014). Fruit nursery paper production process transformation and cost analysis（果树苗圃纸生产流程改造与成本分析）. *Journal of Shaanxi University of Science & Technology*, 32 (04): 1-4.